discrepancy being less than 5% for most of the compounds. The notable exceptions were GaAs, GaP, InP, LiF and TiC but in these cases there was a large spread among the individual temperature factors (47% for GaP).

From the considered data, the recommended values of the temperature factors B^+ and B^- for a given compound are obtained by the weighted average of the individual values given by the different authors, the weight w_i being $1/\sigma_i^2$, where σ_i is the error for an individual observation. In all cases for which the author did not give the error in the B value, the error assigned to this B is defined as $\sigma_i = B_i\rho$, where ρ is the maximum percentage error found in a given set of data and B_i is the temperature factor without the error. The recommended values of the average temperature factors $\bar{B}$ are obtained from the recommended values of B^+ and B^- using the relation

$$\bar{B} = (m^+B^+ + m^-B^-)/(m^+ + m^-), \qquad (4)$$

where m^+ and m^- are the masses of the cation and anion, respectively. The recommended value of the corresponding Debye temperature was calculated using (3) with T the room temperature. The recommended values of the temperature factors B^+, B^- and $\bar{B}$ and the Debye temperature Θ for the 52 compounds are given in Table 1.

It is expected that the heavier of the two atoms in a compound should have a smaller B value. This is indeed the case for most of the compounds. However, for certain compounds (*e.g.* AgBr, CuCl, HgSe, InAs, TlCl, PbS, PbTe and ZnS) it is observed that the heavier atom has a larger B value than that of the lighter atom. This is not surprising because, in the harmonic approximation and for $T > \Theta$, the mean square displacements are independent of the atomic masses (Huiszoon & Groenewegen, 1972; Jex, Mullner & Dyck, 1974). In such cases, the mass dependence of the temperature factors may not be observed.

NMB is grateful to Professor A. Salam for providing facilities at ICTP for part of this work and to SAREC (Sweden) for a financial grant as Senior Associate during his stay at ICPT. Thanks are also due to N. H. March, G. Caglioti, J. Krumhansl, E. Tosatti, Yu Lu, H. Frauenfelder, Gracia Moliner, N. Praveen, P. deGennes, H. Fuess, M. Mullner, P. Weinzierl and O. Eder for many useful discussions. We are also grateful to our colleague Mr M. Siddique for help in this work.

References

BEG, M. M., ASLAM, J., BUTT, N. M., KHAN, Q. H. & ROLANDSON, S. (1974). *Acta Cryst.* A**30**, 662-667.

BUTT, N. M., BASHIR, J., WILLIS, B. T. M. & HEGER, G. (1988). *Acta Cryst.* A**44**, 396-398.

HUISZOON, C. & GROENEWEGEN, P. P. M. (1972). *Acta Cryst.* A**28**, 170-172.

INTERNATIONAL UNION OF CRYSTALLOGRAPHY (1985). *Acta Cryst.* B**41**, 374.

JAMES, R. W. (1967). *The Optical Principles of the Diffraction of X-rays.* London: Bell.

JEX, H., MULLNER, M. & DYCK, W. (1974). *Phys. Status Solidi B*, **61**, 241-246.

STEVENSON, A. W. & HARADA, J. (1983). *Acta Cryst.* A**39**, 202-207.

SUORTTI, P. & JENNINGS, L. D. (1977). *Acta Cryst.* A**33**, 1012-1027.

WILLIS, B. T. M. & PRYOR, A. W. (1975). *Thermal Vibrations in Crystallography.* Cambridge Univ. Press.

Acta Cryst. (1993). A**49**, 174-183

X-ray Integrated Intensities from Semiconductor Substrates and Epitaxic Layers – a Comparison of Kinematical and Dynamical Theories with Experiment

BY ANDREW W. STEVENSON

CSIRO Division of Materials Science & Technology, Locked Bag 33, *Clayton, Victoria* 3168, *Australia*

(*Received* 7 *April* 1992; *accepted* 7 *July* 1992)

Abstract

X-ray integrated intensities have been collected from extended-face specimens as a function of azimuthal angle ψ (rotation angle about the scattering vector) with a four-circle diffractometer for a number of semiconductor substrate materials and epitaxic layers. The Bragg reflections (and X-ray wavelengths) have been chosen so that as wide a range of asymmetry as possible is encompassed. It is shown that the interpretation of these results, in terms of kinematical and perfect-crystal dynamical X-ray diffraction theories, provides a measure of the perfection of the crystal being investigated. The interpretation of some results requires consideration of extinction effects and their dependence on asymmetry. Such

0108-7673/93/010174-10$06.00

measurements, taken from epitaxic layers or substrates beneath epitaxic layers, can also be used to determine the layer thickness and/or identify the composition of a layer.

Introduction

X-ray diffraction techniques have proved to be extremely useful in nondestructively characterizing semiconductor single-crystal substrates and the crystalline layers grown on them by, for example, metal organic chemical vapour deposition (MOCVD) and molecular-beam epitaxy (MBE). High-resolution techniques such as double-crystal diffractometry and topography can provide a wealth of information on the nature, microstructure, quality and uniformity of these crystalline samples (see, for example, Macrander, 1988; Tanner, 1989). In the case of multilayer or superlattice samples, X-ray techniques can yield information on individual layer thicknesses and composition, sharpness of interfaces, strain and the presence of imperfections. The Bond method, for example, can be used to obtain extremely accurate lattice-parameter values (Bond, 1960). Triple-crystal diffractometry can be used to examine the intensity distribution in the vicinity of Bragg peaks in even greater detail than with double-crystal rocking-curve measurements. The advent of synchrotron-radiation sources has increased the potential of the above-mentioned and other X-ray diffraction characterization techniques and created quite new possibilities.

We have recently made extensive use of a computer-controlled four-circle X-ray diffractometer in our characterization of a variety of semiconductor samples (Stevenson, Wilkins, Kwietniak & Pain, 1989; Stevenson & Pain, 1990*a*,*b*; Stevenson, Gao, Pain & Wieluński, 1991). Although the conventional four-circle diffractometer is not a suitable instrument for measuring high-resolution rocking curves, for example, it is extremely useful for measuring integrated intensities. The fact that the ω and 2θ circles are uncoupled enables us to collect data at asymmetric settings. [The symmetric settings of a given Bragg reflection corresponding to the azimuthal angle ψ being 0 or 180°, where we refer to extended-face crystal geometry (Mair, Prager & Barnea, 1971*a*,*b*; Freeman, Mair & Barnea, 1977) and align the sample normal to be accurately parallel to the diffractometer φ axis.] In this paper we will utilize this capability of the four-circle diffractometer to collect accurate X-ray integrated intensities as a function of ψ, for a number of semiconductor substrate materials and epitaxic layers.

The analysis and interpretation of the integrated-intensity results, in terms of kinematical and perfect-crystal dynamical X-ray diffraction theories, provides a test of the theories for a large range of asymmetry. The data presented have been collected at several X-ray wavelengths, which provides a further test of theory, there being, for example, large changes in absorption for a given material, with a concomitant variation of X-ray path length and depth of penetration in the crystal (when absorption is important relative to extinction). By use of different structure factors, wavelengths and degrees of asymmetry, we can essentially alter the sensitivity of the data to the crystalline perfection of the sample (Wooster & Macdonald, 1948; Hirsch & Ramachandran, 1950). The fact that some of the materials studied are neither ideally imperfect nor ideally perfect is also demonstrated and the discrepancy between theory and experiment is discussed in terms of extinction. We will also investigate the dependence of extinction effects on asymmetry, in accordance with the philosophy of Mathieson (1976, 1977, 1979), who identified the asymmetric limits as being extinction-free limits. Hirsch & Ramachandran (1950) studied theoretically the variation of X-ray integrated intensities with asymmetry, structure factor and wavelength for perfect and mosaic crystals.

Theory

The samples studied in this paper are all assumed to be perfectly flat with uniform thickness and to have a surface sufficiently large that the entire incident X-ray beam is intercepted at all azimuthal positions of concern. The samples, in some instances, may not satisfy the usual definition of an extended-face crystal, however, in that the thickness may not be sufficient to neglect transmission of the X-ray beam through to the 'back' of the sample. Our calculations will, therefore, not assume that the sample is infinitely thick unless this is justifiable.

Fig. 1 depicts Bragg reflection occurring from a sample (*a*) with negative asymmetry, (*b*) symmetrically and (*c*) with positive asymmetry. It is convenient to define two quantities, α and β, as follows:

$$\alpha = -\tan^{-1}(\sin\psi/\tan\chi_0) = \omega - \theta_B \qquad (1)$$

and

$$\beta = \cot\theta_B \tan\alpha, \qquad (2)$$

where χ_0 is the value of the diffractometer angle χ where $\psi = 0$ and θ_B is the Bragg angle. The conventions for our four-circle diffractometer angles (2θ, ω, χ and φ) and the azimuthal angle ψ are given by Stevenson & Pain (1990*a*). The quantity α represents the angle between the crystal surface and the Bragg planes in the horizontal or diffraction plane. In the case of negative asymmetry (Fig. 1*a*), $\alpha < 0$, $\beta < 0$, $\omega < \theta_B$ and $0 < \psi < 180°$. In the case of positive asymmetry (Fig. 1*c*), $\alpha > 0$, $\beta > 0$, $\omega > \theta_B$ and $-180° < \psi < 0$. Finally, the symmetric aspects (Fig. 1*b*) correspond to $\alpha = 0$, $\beta = 0$, $\omega = \theta_B$ and $\psi = 0$ or 180°. For a parallel incident X-ray beam of width (in the diffraction

plane) W, the diffracted X-ray beam width can be approximated by W/b, where

$$b = \sin(\theta_B + \alpha)/\sin(\theta_B - \alpha) \quad (3)$$

and the size of the beam on the crystal face (in the diffraction plane) is $W/\sin(\theta_B + \alpha)$. The effect of asymmetry on Bragg reflection from perfect crystals has been discussed by, for example, Wilkins (1978*a*).

The integrated intensity for an ideally imperfect crystal with the relevant geometry can be given [in kinematical theory; see, for example, James (1948)] by

$$I_{\text{kin}} = |F_H|^2 LPA_H S\lambda^3, \quad (4)$$

where F_H is the structure factor for Bragg reflection H (Miller indices h, k, l), L is the Lorentz factor, P is the polarization factor, A_H is the transmission factor, S is the scale factor and λ is the X-ray wavelength. Stevenson & Pain (1990*a*) provided the expression

$$A_H = (\text{cosec}\,\omega)[1 - \exp(-\mu t X \sec\eta)]/\mu X, \quad (5)$$

where μ is the linear absorption coefficient, t is the crystal thickness (measured along the surface normal direction),

$$\sec\eta = (1 - \cos^2\chi_0 \cos^2\psi)^{-1/2} \quad (6)$$

and

$$X = \text{cosec}\,\omega + \text{cosec}\,(2\theta_B - \omega). \quad (7)$$

In the case of a sample of effectively infinite thickness, (5) simplifies to

$$A_H = (\text{cosec}\,\omega)/\mu X, \quad (8)$$

which has the value $1/(2\mu)$ at the symmetric aspects. Another quantity that will prove to be useful is the mean path length in the crystal, given by

$$\bar{T} = -(1/A_H)\,\mathrm{d}A_H/\mathrm{d}\mu$$
$$= 1/\mu + t(\sec\eta)[X - (\text{cosec}\,\omega)/\mu A_H], \quad (9)$$

which simplifies to $1/\mu$ for a sample of effectively infinite thickness.

In the case of the dynamical theory for Bragg reflection with a thick perfect noncentrosymmetric crystal [see, for example, Zachariasen (1945) and Cole & Stemple (1962); we will follow the latter's formalism directly], we define

$$\psi_H = \psi'_H + i\psi''_H, \quad (10)$$

where

$$\psi'_H = -(r_c\lambda^2/\pi V)\sum_j (f_{0j} + f'_j)\exp(2\pi i\mathbf{H}\cdot\mathbf{r}_j) \times \exp(-M) \quad (11)$$

and

$$\psi''_H = -(r_c\lambda^2/\pi V)\sum_j f''_j \exp(2\pi i\mathbf{H}\cdot\mathbf{r}_j) \times \exp(-M), \quad (12)$$

where r_c is the classical electron radius, V is the unit-cell volume and the summations correspond to the familiar subdivisions of F_H. It is then necessary to define

$$\psi'_H = (\psi'_H)_r + i(\psi'_H)_i \quad (13)$$

and

$$\psi''_H = (\psi''_H)_r + i(\psi''_H)_i, \quad (14)$$

where the real and imaginary components have been separated. We can then obtain the reflectivity curve (reflecting power)

$$R = \{(1 + \kappa^2 + 2s)/[(1 - \kappa^2)^2 + 4p^2]^{1/2}\} \times [L - (L^2 - 1)^{1/2}], \quad (15)$$

where

$$L = \{y^2 + g^2 + [(y^2 - g^2 - 1 + \kappa^2)^2 + 4(gy - p)^2]^{1/2}\}/[(1 - \kappa^2)^2 + 4p^2]^{1/2}, \quad (16)$$

$$\kappa = |\psi''_H|/|\psi'_H|, \quad (17)$$

$$s = [(\psi'_H)_i(\psi''_H)_r - (\psi'_H)_r(\psi''_H)_i]/|\psi'_H|^2, \quad (18)$$

$$p = [(\psi'_H)_r(\psi''_H)_r + (\psi'_H)_i(\psi''_H)_i]/|\psi'_H|^2, \quad (19)$$

$$y = [(1 + b)\psi'_0/2 + b(\theta - \theta_B)\sin 2\theta_B]/(b^{1/2}K|\psi'_H|) \quad (20)$$

and

$$g = (1 + b)(\psi''_0/2)/(b^{1/2}K|\psi'_H|), \quad (21)$$

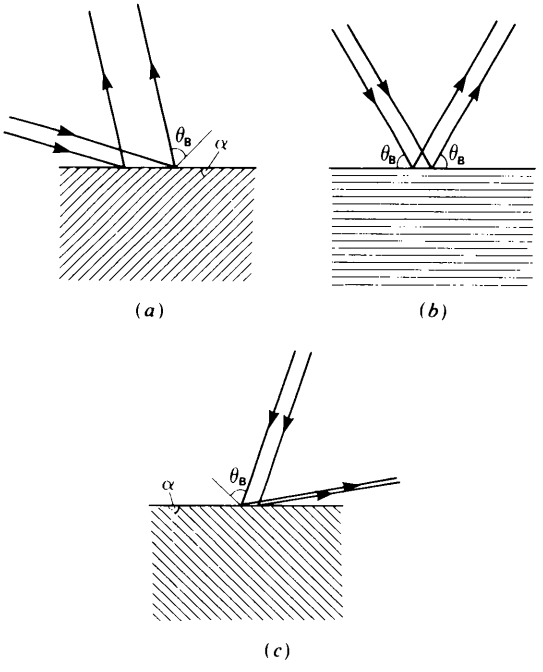

Fig. 1. Bragg reflection occurring from a sample (*a*) with negative asymmetry, (*b*) symmetrically and (*c*) with positive asymmetry.

K being 1 for the normal component of polarization and $|\cos 2\theta_B|$ for the parallel component. For a centrosymmetric crystal, $\psi'_H = (\psi'_H)_r$, $\psi''_H = (\psi''_H)_r$, $s = 0$ and $p = \kappa$.

In the case of the dynamical theory for Bragg reflection with a thin perfect crystal, we follow the formalism of Wilkins (1978*b*) (see also Zachariasen, 1945),

$$R = b|\psi_H|^2 K^2(\sin^2 av + \sinh^2 aw)/D, \quad (22)$$

where

$$D = |q + z^2| + (|q + z^2| + |z|^2)\sinh^2 aw - (|q + z^2| - |z|^2)\sin^2 av + \mathrm{Re}(-z^* u) \times \sinh 2aw + \mathrm{Im}(z^* u)\sin 2av, \quad (23)$$

$$u \equiv v + iw \equiv (q + z^2)^{1/2}, \quad (24)$$

$$q = -b\psi_H \psi_{\bar{H}} K^2, \quad (25)$$

$$z = (1 + b)\psi_0/2 + b(\theta - \theta_B)\sin 2\theta_B \quad (26)$$

and

$$a = \pi t(\sec \eta)(\mathrm{cosec}\, \omega)/\lambda, \quad (27)$$

z^* being the complex conjugate of z and $\mathrm{Re}(Y)$ and $\mathrm{Im}(Y)$ representing respectively the real and imaginary components of the complex quantity Y.

Experimental

It has been implicitly assumed in the foregoing discussion that the incident X-ray beam is parallel and monochromatic. The four-circle diffractometer used for the measurements presented in this paper is not equipped with an incident-beam monochromator. All integrated intensities have been collected with the entire $K\alpha$ doublet (in some cases the appropriate $K\beta$ filter has been used). Although the X-ray beam used is basically divergent, we have used X-ray tubes disposed to give a line focus that is only 35 μm wide (in the diffraction plane) as viewed from the crystal centre (for a 5° take-off angle). The incident-beam collimator provides a circular aperture of diameter 140 μm, resulting in a beam divergence (for an effective point source located at a larger distance from the sample than the real source) in the diffraction plane of approximately 191″ (115″) for the penumbra (umbra). These rather stringent conditions are also necessary to limit the area of crystal irradiated at the extremes of negative asymmetry [see Fig. 1 and (3)]. In such cases it is also necessary to ensure that any detector aperture being used is capable of receiving the entire (quasiparallel) signal. It can be shown that the effect of not having an ideal incident X-ray beam (*i.e.* neither parallel nor monochromatic) is unimportant in the present circumstances and in particular where the measured quantity is the integrated intensity.

Each sample was initially aligned so that the sample normal and diffractometer φ axis were accurately parallel (to better than 0.05°) by use of a laser technique (Moss & Barnea, 1976). Integrated intensities were collected using $\omega/2\theta$ scans, with a minimum step size of 0.005° in ω, at 293 K. Measurements were, in certain cases, repeated at various generator settings to check on the efficacy of the dead-time corrections.

Data were collected for four samples: (i) Si, effectively infinite thickness for all wavelengths and Bragg reflections used, approximately (111) orientation; (ii) GaAs, effectively infinite thickness, approximately (100) orientation; (iii) GaAs, effectively infinite thickness, approximately (311) orientation, an approximately 1 μm layer of $Hg_{1-x}Cd_xTe$ (311) had been deposited on the surface by MOCVD; (iv) CdTe, nominally 8.15 μm thick, approximately (111) orientation; this layer was deposited on a sapphire substrate. Accurate orientation (UB) matrices were obtained for each sample [to enable azimuthal positions to be selected reliably - Bragg reflections were also optimized (with φ fixed) prior to measurement]. Polarity determinations were made for each of the noncentrosymmetric structures (GaAs and CdTe), as discussed by Stevenson, Wilkins, Kwietniak & Pain (1989).

We have endeavoured, for a given Bragg reflection, to collect the integrated intensity data over the full range of ψ, from the symmetric aspect $\psi = -180°$ ($\alpha = 0$), to the extreme of positive asymmetry $\psi = -90°$ ($\alpha = 90° - \chi_0$), to the symmetric aspect $\psi = 0$ ($\alpha = 0$), to the extreme of negative asymmetry $\psi = 90°$ ($\alpha = \chi_0 - 90°$) and to the symmetric aspect $\psi = 180°$ (identical to $\psi = -180°$, of course).* The only reasons for not collecting the data for a particular value of ψ are in the event that multiple-diffraction effects obtrude or if the reflection is not physically accessible for that ψ (owing to, for example, the χ circle obscuring the detector). The Bragg reflections and X-ray wavelengths were chosen so as to encompass as wide a range of asymmetry as possible (in practice) and, as such, are special. The value of ω at $\psi = 90°$ (or $2\theta_B - \omega$ at $\psi = -90°$) was typically around 3° (minimum value 1.7°). The value of $-\beta$ at $\psi = 90°$ (or β at $\psi = -90°$) was typically around 0.9 (maximum value 0.93). These degrees of asymmetry do not warrant a consideration of total-external-reflection effects, *i.e.* the glancing angles used are not yet at the critical angle (the largest critical-angle value encountered here being 0.46°).

Analysis

To carry out the calculations presented in the next section we have used the atomic scattering factors of

* The extremes of asymmetry mentioned here are not, in general, the asymmetric limits mentioned by, for example, Mathieson (1976), where $\alpha = \pm\theta_B$ ($\beta = \pm 1$, $\omega - \theta_B = \pm\theta_B$), which correspond to the diffracted or incident X-ray beams being parallel to the crystal surface.

Doyle & Turner (1968) and the anomalous-dispersion corrections of Cromer & Liberman (1970). The Debye–Waller factors used in the harmonic temperature factors are from Prager (1971) for Si and from Reid (1983) for GaAs and CdTe. Anharmonic thermal vibrations and bonding effects are not considered. Thermal-diffuse-scattering corrections to measured integrated intensities were also ignored. The lattice parameters used were 5.4309 Å for Si (National Bureau of Standards, 1976), 5.6538 Å for GaAs (ASTM Card No. 32-665) and 6.481 Å for CdTe (National Bureau of Standards, 1964). Linear absorption coefficients were calculated from mass attenuation coefficients given in *International Tables for X-ray Crystallography* (1974).

Since the incident X-ray beams used were unpolarized, calculations were, in general, made for both polarization components and averaged. All least-squares refinements were carried out with unit weights.

Results and interpretation

Silicon

Figs. 2, 3 and 4 show integrated intensities plotted as a function of ψ for the Mo $K\alpha$ 551, Co $K\alpha$ 113 and Cr $K\alpha$ 220 Bragg reflections, respectively. In each case, the kinematical calculations were made with use of (4)–(7), the dynamical calculations with (1), (3) and (11)–(21). At each ψ value the dynamical reflectivity curve is calculated and then integrated. Fig. 5 shows, by way of example, the calculated reflectivity curves for the Cr $K\alpha$ 220 reflection at $\psi = 0$ and $\pm 90°$. In Figs. 2–4 the dynamical theory results have been scaled to unity at $\psi = 0$ and the kinematical theory and experimental results scaled to agree with the dynamical theory result at $\psi = 90°$. (We note that the theoretical results are not constrained to agree at

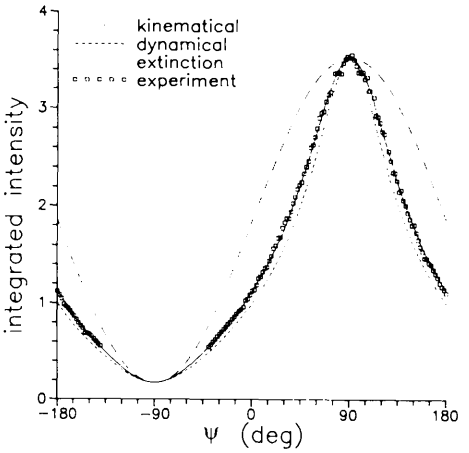

Fig. 3. Integrated intensities as a function of ψ for the Co $K\alpha$ 113 Bragg reflection from Si.

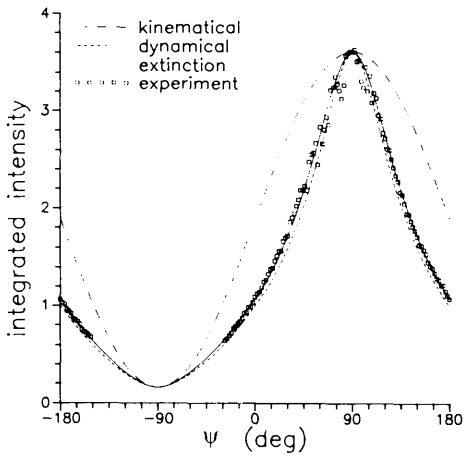

Fig. 4. Integrated intensities as a function of ψ for the Cr $K\alpha$ 220 Bragg reflection from Si.

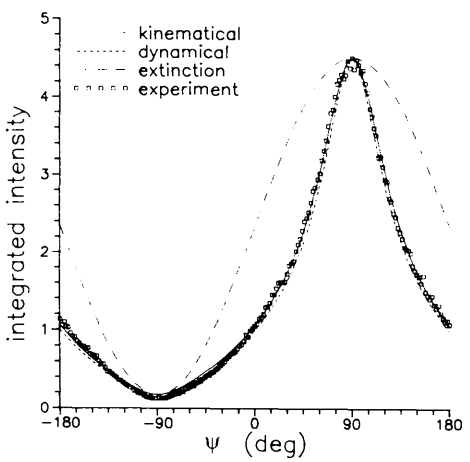

Fig. 2. Integrated intensities as a function of ψ for the Mo $K\alpha$ 551 Bragg reflection from Si.

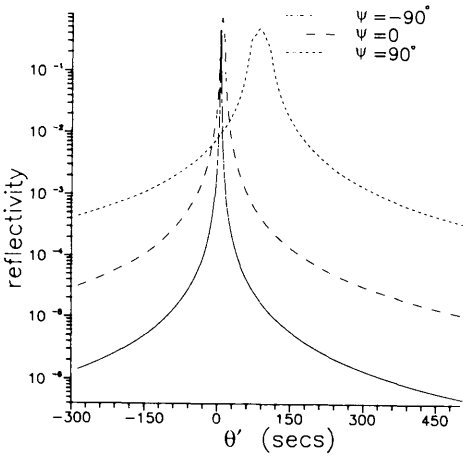

Fig. 5. Calculated reflectivity curves (dynamical theory) for the Cr $K\alpha$ 220 Bragg reflection from Si as a function of θ', the deviation from θ_B.

Table 1. *Details of the* Si *and* GaAs *data*

The refined parameter values obtained from consideration of the presence of extinction effects (ε) are included together with a measure of the least-squares fit (Hamilton's R factor, R_H). Values of the level of interaction parameter at $\psi = 0$ and $\pm 90°$ are also included.

Material	*hkl*	λ	ε	R_H (%)	$1/g\ (\psi = 0)$	$1/g\ (\psi = \pm 90°)$
Si	551	Mo $K\alpha$	0.434 (5)	2.87	−31.4	−12.1
Si	113	Co $K\alpha$	0.720 (3)	1.30	−9.2	−3.9
Si	220	Cr $K\alpha$	0.781 (11)	3.61	−8.2	−3.3
GaAs	$51\bar{1}$	Mo $K\alpha$	1.13 (2)	2.11	−5.3	−3.0
GaAs	$31\bar{1}$	Cu $K\alpha$	0.999 (10)	1.83	−12.7	−4.7

$\psi = -90°$.) It is clear from Figs. 2-4 that the experimental data are in much better agreement with dynamical theory, compared with kinematical theory. Given the perfection of the material involved (Si), this is not surprising. However, there is clearly a discrepancy with dynamical theory for all three cases.

We initially investigated the possibility of the presence of a nondiffracting surface layer (*e.g.* SiO_2). The effect of such a layer, with the assumption of a uniform thickness t' (measured along the surface-normal direction) and a linear absorption coefficient μ', would be that the theoretical integrated intensity should be multiplied by a factor

$$f = \exp(-\mu' t' X \sec \eta). \tag{28}$$

Least-squares refinements were carried out using (28) in conjunction with the dynamical theory calculations (refining $\mu' t'$). We found that the experimental data in Figs. 2-4 could indeed be fitted very well in this way. However, the refined values of $\mu' t'$ proved to be quite unacceptable in that the observed wavelength dependence could not be explained. For example, if we assume that the proposed layer has the same linear absorption coefficient as the bulk ($\mu' = \mu$), the derived values of t' are 1.83 (9), 0.266 (4) and 0.081 (5) μm for Figs. 2, 3 and 4, respectively. Considering other possible layers, such as SiO_2, does not resolve this anomaly.

The second possibility is to attribute the remaining discrepancy between dynamical theory and experiment or, more correctly, the discrepancy between kinematical theory and experiment, to extinction. We begin by considering the familiar expression for the primary-extinction factor for the infinite parallel plate (Darwin 1922; Zachariasen, 1945), which should multiply I_{kin} [see (4)],

$$y = (\tanh A)/A, \tag{29}$$

where

$$A = r_e \lambda |F_H| K t (\sec \eta)/\{V[\sin \omega \sin(2\theta_B - \omega)]^{1/2}\}. \tag{30}$$

In the present case, our Si sample is of effectively infinite thickness. If we replace t in (30) by the depth of penetration of the X-ray beam (measured in the surface-normal direction) corresponding to a path length of $\bar{T} = 1/\mu$ [see (9)], we get

$$A = \frac{r_e \lambda |F_H| K}{\mu V} \frac{[\text{cosec } \omega \text{ cosec } (2\theta_B - \omega)]^{1/2}}{[\text{cosec } \omega + \text{cosec } (2\theta_B - \omega)]}. \tag{31}$$

For symmetric aspects, (31) simplifies to

$$A = r_e \lambda |F_H| K/(2\mu V), \tag{32}$$

and for the asymmetric limits ($\omega = 0$ and $\omega = 2\theta_B$), $A = 0$ and $y = 1$, *i.e.* these asymmetric limits are extinction-free, as discussed by Mathieson (1976, 1977, 1979).

Least-squares refinements were performed by variation of a dimensionless parameter ε that multiplied A [see (31)]. We do not assign any physical meaning to the parameter ε. Table 1 shows the results obtained for Si; Figs. 2-4 include the theoretical curves (solid lines) generated in this way (and scaled as for the kinematical calculations). Table 1 includes values of Hamilton's R factor, R_H (Hamilton, 1965), as a measure of the fit. These values and the figures indicate that the Si data are fitted very well. It is important to appreciate, however, that (29) and (31) can only be treated as an empirical extinction correction for the Si data. We cannot justify (31) theoretically because Darwin's formula [(29)] is based on negligible absorption, whereas we have set the effective crystal thickness at a value dictated by absorption rather than extinction. The theoretical validity of the form of (31) is the subject of further study. The fits obtained for the Si data presented here are all the more remarkable when one considers that there is a 30-fold change in the linear absorption coefficient, from 15.2 cm^{-1} for Mo $K\alpha$ to 472.3 cm^{-1} for Cr $K\alpha$. To compare the degree of absorption *versus* extinction, we have included in Table 1 values of the level of interaction parameter at $\psi = 0$ and $\pm 90°$ [see Wilkins (1978*a*) and (21)],

$$1/g = (1 - \beta^2)^{1/2} K |\psi'_H|/\psi''_0. \tag{33}$$

Physically, $1/g$ gives a measure of the degree of extinction relative to the degree of absorption. Hirsch & Ramachandran (1950) give the result $-1/g \simeq 4t_{\text{abs}}/t_{\text{ext}}$, where t_{abs} (t_{ext}) is the absorption (extinction) length in the absence of diffraction (absorption). The values of $1/g$ for $\psi = 0$ reflect the dominance of

extinction effects. However, at our extremes of asymmetry ($\psi = \pm 90°$), extinction and absorption effects are, in general, comparable.

Fig. 6 shows the calculated extinction factors for the three Si reflections as a function of β. The maximum extinction effect occurs at the symmetric aspects ($\beta = 0$); the asymmetric limits ($\beta = \pm 1$) are seen to be extinction-free (Mathieson, 1976, 1977, 1979).

Gallium arsenide (1)

Figs. 7 and 8 show integrated intensities plotted as a function of ψ for the Mo $K\alpha$ $51\bar{1}$ and Cu $K\alpha$ $31\bar{1}$ Bragg reflections from GaAs, respectively. The experimental data and calculations are presented as described already for Si. Although the experimental data are very close to the dynamical theory curves, there is still a discrepancy in Fig. 7 at least. As for Si, we cannot explain this discrepancy in terms of a nondiffracting surface layer and have carried out an extinction correction using (29) and (31). The results are included in Table 1 and Figs. 7 and 8. We see that the refined values of ε are both very close to unity and the experimental data are fitted very well. The linear absorption coefficients for Mo $K\alpha$ and Cu $K\alpha$ are very similar, 328 and 368 cm^{-1}, respectively, owing to the presence of the K-absorption edges. Fig. 9 shows the corresponding calculated extinction factors as a function of β.

Gallium arsenide (2)

Fig. 10 shows integrated intensities plotted as a function of ψ for the Mo $K\alpha$ $7\bar{1}3$ Bragg reflection from GaAs (this sample being the one with a deposited MOCVD-grown $Hg_{1-x}Cd_xTe$ layer). The experimental data and calculations are presented as previously described. Both theoretical curves include the effect of absorption in the nondiffracting

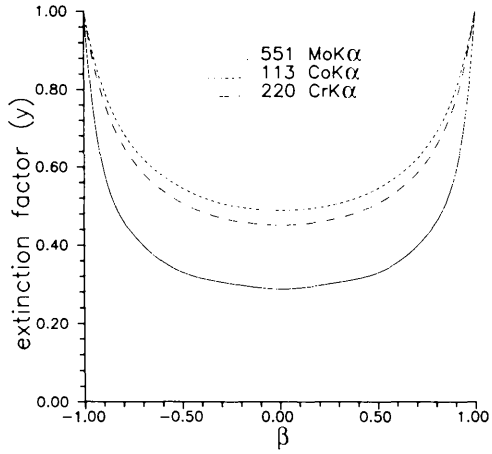

Fig. 6. Calculated extinction factors for the three Si reflections (Figs. 2, 3 and 4) as a function of β.

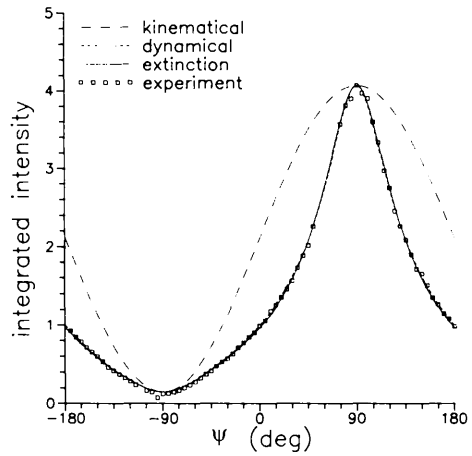

Fig. 8. Integrated intensities as a function of ψ for the Cu $K\alpha$ $31\bar{1}$ Bragg reflection from GaAs.

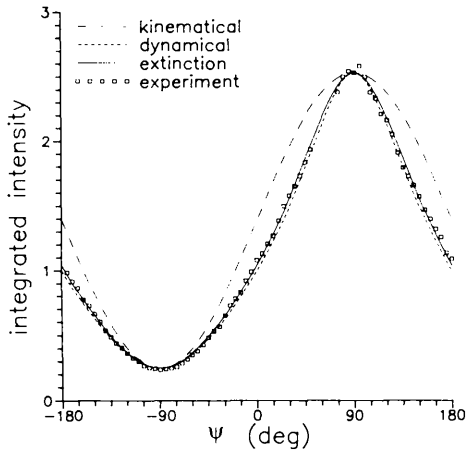

Fig. 7. Integrated intensities as a function of ψ for the Mo $K\alpha$ $51\bar{1}$ Bragg reflection from GaAs.

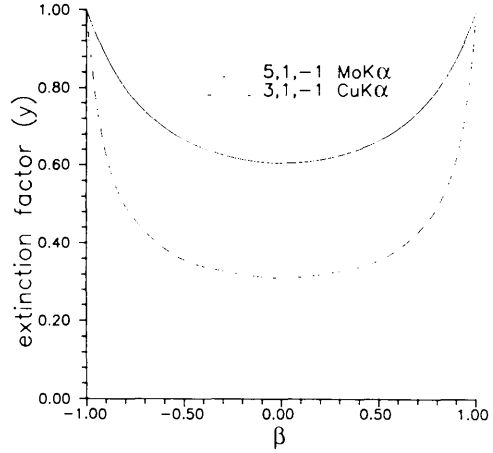

Fig. 9. Calculated extinction factors for the two GaAs reflections (Figs. 7 and 8) as a function of β.

$Hg_{1-x}Cd_xTe$ layer by use of (28). Least-squares refinements (refining $\mu't'$) favoured the dynamical calculations rather than the kinematical calculations, the respective values of R_H being 3.19 and 4.34%. The refined value of $\mu't'$ (for the dynamical calculations) was 0.0718 (3). The sample being studied here is the sample denoted *S*1 by Stevenson, Gao, Pain & Wieluński (1991) and the value of $\mu't'$ obtained by these authors (for Mo $K\alpha$ radiation) was 0.073 (9) [$\mu' = 539.7\ cm^{-1}$ and $t' = 1.36\ (12)\ \mu m$], in excellent agreement with the present case.

Fig. 10 demonstrates the possibilities for using such measurements to determine t' and identify the composition of a layer material, *e.g.* obtaining a value for the Cd fraction x in the present case. If the layer material is known, one set of measurements will yield a value for t'. If the composition of the layer is not known, two or more sets of measurements, collected with different X-ray wavelengths, may enable t' to be determined and some estimate of the layer composition to be made (this may prove easier if the X-ray wavelengths encompass absorption edges of the layer material).

The dip at $\psi = 90°$ in Fig. 10 is attributed to the absorption (path length) of the X-ray beam in the layer being a maximum (as it also is at $\psi = -90°$). If the degree of asymmetry is sufficiently large, for the X-ray wavelength in question, the X-ray beam may effectively fail to reach the substrate through a deposited layer. Fig. 11 demonstrates this point; it shows integrated intensities plotted as a function of ψ for the Cr $K\alpha$ 202 Bragg reflection from the GaAs substrate. Because of the nature of the curves in Fig. 11, the experimental data and kinematical theory results have been scaled to unity at $\psi = 0$ (rather than to agree with the dynamical theory results at $\psi = 90°$). The values of $\mu't'$ used for the kinematical and dynamical calculations in Fig. 11 were based on the refined values of $\mu't'$ for the respective curves in Fig. 10.

Cadmium telluride

The motivation for studying this thin CdTe layer is that we believe it should be relatively imperfect, in contrast with the Si and GaAs crystals already investigated. Figs. 12 and 13 show integrated intensities plotted as a function of ψ for the Mo $K\alpha$ 624 and Cr $K\alpha$ 311 Bragg reflections, respectively. In each case, the kinematical calculations were made by use of (4)-(7) and the dynamical calculations were made by use of (1), (3), (6), (10)-(12) and (22)-(27). At each ψ value, the dynamical reflectivity curve is calculated and then integrated. Fig. 14 shows the calculated reflectivity curves for the Mo $K\alpha$ 624 reflection at $\psi = 0$ and $\pm 90°$. The scaling of the results in Figs. 12 and 13 is as described for Figs. 2-4.

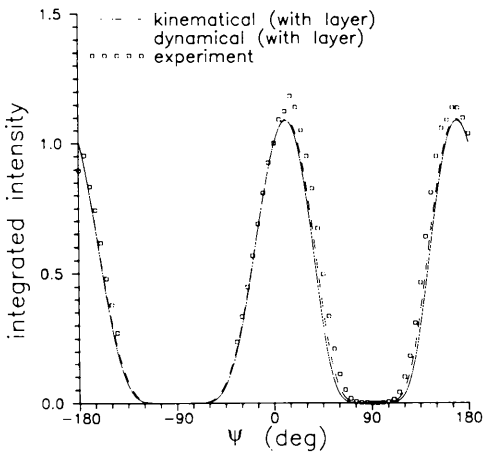

Fig. 11. Integrated intensities as a function of ψ for the Cr $K\alpha$ 202 Bragg reflection from GaAs (through an $Hg_{1-x}Cd_xTe$ layer).

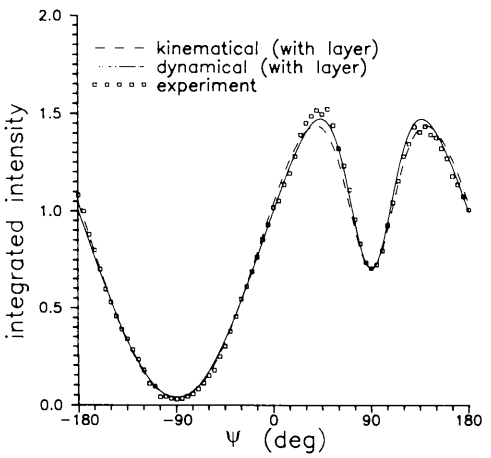

Fig. 10. Integrated intensities as a function of ψ for the Mo $K\alpha$ $7\bar{1}3$ Bragg reflection from GaAs (through an $Hg_{1-x}Cd_xTe$ layer).

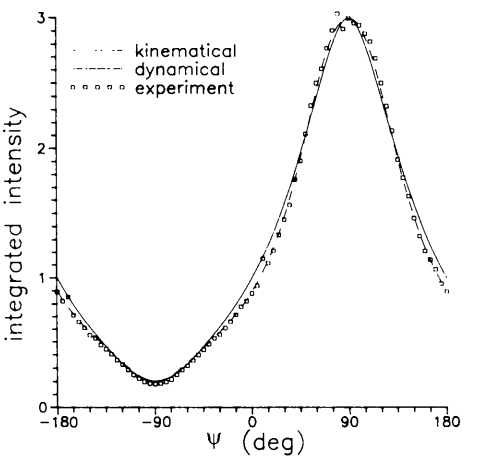

Fig. 12. Integrated intensities as a function of ψ for the Mo $K\alpha$ 624 Bragg reflection from CdTe.

Clearly, the experimental data are in considerably better agreement with the kinematical curves in Figs. 12 and 13 than in other figures, with no evidence for significant extinction effects being present. We note that the differences between the kinematical and dynamical calculations in Figs. 12 and 13 are relatively small. We attribute this to the reduced importance of multiple interferences in the thin-layer sample.

Concluding remarks

Accurate X-ray integrated intensities, collected as a function of asymmetry and wavelength, for a number of semiconductor materials (including thin epitaxic layers) have been interpreted very successfully in terms of kinematical and perfect-crystal dynamical X-ray diffraction theories. In certain instances, attempts have been made to include extinction effects to account for remaining discrepancies between theory and experiment. The experimental results have been shown to be in accord with theory over a very wide range of asymmetry and in a consistent manner for a variety of wavelengths, which encompass quite large changes in absorption.

The interpretation of the results presented here provides a measure of the perfection of the crystal in question and, to some extent, of the uniformity of the sample with depth, *via* different penetration depths for the different asymmetries and X-ray wavelengths. The empirical extinction corrections used are shown to have an asymmetry dependence consistent with the philosophy of Mathieson (1976, 1977, 1979), who identified the asymmetric limits as being extinction-free limits.

It has been shown that measurements such as those presented here can be used to determine the thickness of surface or deposited layers (see, for example, Mathieson, 1975), diffracting from either the layer itself or from the underlying substrate material. In certain circumstances, the use of multiwavelength X-ray data may also provide a means of identifying the composition of a layer.

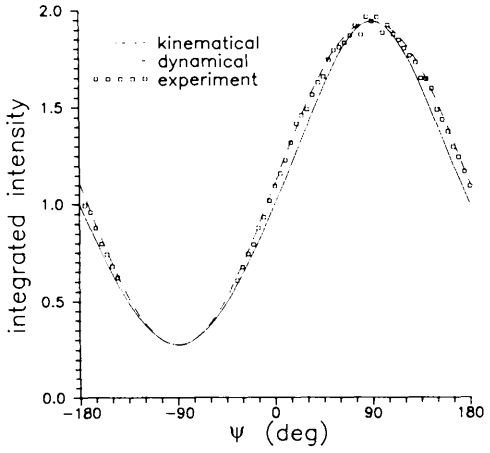

Fig. 13. Integrated intensities as a function of ψ for the Cr $K\alpha$ 311 Bragg reflection from CdTe.

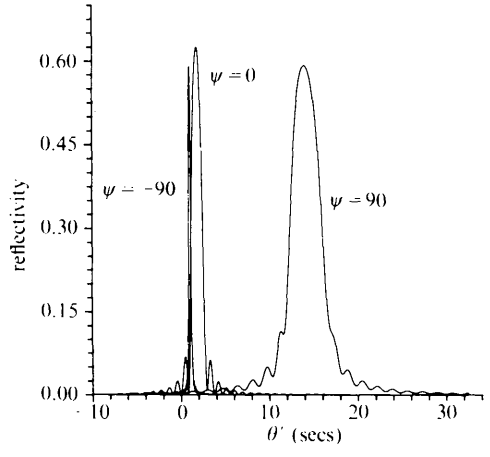

Fig. 14. Calculated reflectivity curves (dynamical theory) for the Mo $K\alpha$ 624 Bragg reflection from CdTe as a function of θ', the deviation from θ_B.

I am grateful to Professors A. McL. Mathieson and T. M. Sabine and to Drs S. W. Wilkins and T. J. Davis for valuable discussions. I would also like to express my appreciation to Drs G. N. Pain and T. J. Davis and to Mr P. L. Francis for supplying samples and helping with sample preparation. Support was provided under the Generic Technology component of the Industry, Research and Development Act, 1986 (Grant nos. 15019 and 15052).

References

BOND, W. L. (1960). *Acta Cryst.* **13**, 814-818.
COLE, H. & STEMPLE, N. R. (1962). *J. Appl. Phys.* **33**, 2227-2233.
CROMER, D. T. & LIBERMAN, D. (1970). *J. Chem. Phys.* **53**, 1891-1898.
DARWIN, C. G. (1922). *Philos. Mag.* **43**, 800-829.
DOYLE, P. A. & TURNER, P. S. (1968). *Acta Cryst.* A**24**, 390-397.
FREEMAN, D. K., MAIR, S. L. & BARNEA, Z. (1977). *Acta Cryst.* A**33**, 355-359.
HAMILTON, W. C. (1965). *Acta Cryst.* **18**, 502-510.
HIRSCH, P. B. & RAMACHANDRAN, G. N. (1950). *Acta Cryst.* **3**, 187-194.
International Tables for X-ray Crystallography (1974). Vol. IV. Birmingham: Kynoch Press. (Present distributor Kluwer Academic Publishers, Dordrecht.)
JAMES, R. W. (1948). *The Optical Principles of the Diffraction of X-rays.* London: Bell.
MACRANDER, A. T. (1988). *Annu. Rev. Mater. Sci.* **18**, 283-302.
MAIR, S. L., PRAGER, P. R. & BARNEA, Z. (1971*a*). *Nature (London) Phys. Sci.* **234**, 35.
MAIR, S. L., PRAGER, P. R. & BARNEA, Z. (1971*b*). *J. Appl. Cryst.* **4**, 169-171.
MATHIESON, A. McL. (1975). *Acta Cryst.* A**31**, 769-774.
MATHIESON, A. McL. (1976). *Nature (London)*, **261**, 306-308; **262**, 236.
MATHIESON, A. McL. (1977). *Acta Cryst.* A**33**, 610-617.
MATHIESON, A. McL. (1979). *Acta Cryst.* A**35**, 50-57.

MOSS, G. & BARNEA, Z. (1976). *J. Appl. Cryst.* **9**, 510-511.
National Bureau of Standards (1964). Monograph 25, Section 3, p. 21.
National Bureau of Standards (1976). Monograph 25, Section 13, p. 35.
PRAGER, P. R. (1971). PhD thesis, Univ. of Melbourne, Australia.
REID, J. S. (1983). *Acta Cryst.* A**39**, 1-13.
STEVENSON, A. W., GAO, D., PAIN, G. N. & WIELUŃSKI, L. S. (1991). *Acta Cryst.* A**47**, 128-133.
STEVENSON, A. W. & PAIN, G. N. (1990*a*). *J. Appl. Phys.* **68**, 569-573.
STEVENSON, A. W. & PAIN, G. N. (1990*b*). *Aust. J. Phys.* **43**, 793-799.
STEVENSON, A. W., WILKINS, S. W., KWIETNIAK, M. S. & PAIN, G. N. (1989). *J. Appl. Phys.* **66**, 4198-4200.
TANNER, B. K. (1989). *J. Electrochem. Soc.* **136**, 3438-3443.
WILKINS, S. W. (1978*a*). *Proc. R. Soc. London Ser. A*, **364**, 569-589.
WILKINS, S. W. (1978*b*). *Acta Cryst.* A**34**, 343-344.
WOOSTER, W. A. & MACDONALD, G. L. (1948). *Acta Cryst.* **1**, 49-54.
ZACHARIASEN, W. H. (1945). *Theory of X-ray Diffraction in Crystals*. New York: Wiley.

Acta Cryst. (1993). A**49**, 183-190

On Predicting Scan Profiles: the Nature of the 'Aberration Function'

BY RICCARDO DESTRO

Dipartimento di Chimica Fisica ed Elettrochimica, Università di Milano, Via Golgi 19, *Milano* 20133, *Italy*

AND RICHARD E. MARSH

The Beckman Institute, California Institute of Technology, Pasadena, California* 91125, *USA*

(*Received* 11 *February* 1992; *accepted* 15 *July* 1992)

Abstract

In an earlier treatment [Destro & Marsh (1987). *Acta Cryst.* A**43**, 711-718], an attempt was made to predict the shapes of high-angle θ-2θ scan profiles by convoluting a low-angle profile with the presumedly known spectral distribution function for the incident (crystal-monochromatized Mo $K\alpha$) radiation but it was found necessary to introduce a third component, an 'aberration function', that varied with the Bragg angle θ. It is shown here that the primary purpose of the aberration function is to correct for defects in the spectral-distribution function. In particular, the effective intensity ratio between the $K\alpha_2$ and $K\alpha_1$ spectral lines can apparently deviate greatly (by more than 10%) from the theoretical value of 0.499, depending upon the alignment of the monochromator crystal, and an appreciable amount of white radiation may also be present. By a suitable modification of the spectral-distribution function, high-angle scan profiles can be predicted from accurate measurements of a low-angle profile; as a result, scan-truncation losses can, for the most part, be removed. However, modeling the spectral distribution function appropriate to a particular experiment remains a difficult empirical procedure.

Introduction

The problem of scan truncation in single-crystal diffractometry is well known: at even moderately high Bragg angles, the angular range in a typical θ-2θ scan is usually not large enough, owing to interference with neighboring reflections, to encompass the entire scan profile. Consequently, the tails beyond the scan range are missing from the recorded intensity and the measured backgrounds, being recorded within these tails, are artificially large; if these backgrounds are subtracted from the total scan intensities in the usual way, the net intensities will again be systematically underestimated. It appears that, taken together, these two effects can lead to recorded intensities that are too low, perhaps by 15% at $2\theta = 40°$ (Destro & Marsh, 1987; hereinafter, DM).

In an attempt to arrive at a simple procedure for estimating the amount of this 'truncation loss' in a particular experiment, DM considered the possibility that the entire scan profile at any Bragg angle might be predicted from a single profile measured at a very low angle (where the entire profile can be captured). In this development, DM first presumed that the intensity profile at any angle is a combination (a convolution) of two components: (1) a known θ-dependent component, representing the emission spectrum of the incident radiation; and (2) an unknown θ-independent component, reflecting other characteristics of the incident beam and the size and mosaicity of the diffracting crystal. In principle, this second, θ-independent, component (which DM called the 'basic profile') could be derived by deconvoluting, from a measured low-angle profile, the emission spectrum appropriate to that angle; indeed, at a low enough angle ($2\theta < 10°$ or so), the emission spectrum would be close enough to a delta function

* Contribution No. 8573.

0108-7673/93/010183-08$06.00